Computing Binary Scattering and Breakup in Three-Body System

P. A. Belov, E. R. Nugumanov and S. L. Yakovlev

Department of Computational Physics, St. Petersburg State University, 1 Ulyanovskaya st., Saint-Petersburg 198504, Russia

Abstract

Two approaches for computing binary and breakup amplitudes for three-body scattering above the breakup threshold are presented. The asymptotic approach provides a way to take into account the orthogonality of the binary and breakup channels. It reduces the problem to a boundary value problem with known inhomogeneous boundary conditions. The scattering amplitudes are calculated without reconstruction of the solution over the entire configuration space. The complex-scaling method reduces the scattering problem to a boundary value problem with homogeneous zero boundary conditions. It allows calculating the amplitudes via an integral representations. Both methods are applied to neutron-deuteron scattering. The binary and breakup amplitudes are calculated using a developed parallel algorithm.

Keywords: *Three-body systems; Faddeev equations; binary amplitude; breakup amplitude; asymptotic approach; complex-scaling method; domain decomposition method*

1 Introduction

Study of three-body scattering problems includes developing reliable analytical approaches as well as effective computational techniques. One of the approaches for treating neutron-deuteron (nd) scattering above the breakup threshold is based on the three-body configuration space Faddeev formalism [1]. The differential Faddeev equations are reduced to a boundary value problem by implementing appropriate boundary conditions. The existing boundary conditions have been introduced by S. P. Merkuriev [2]. In this paper we continue developing the boundary value problem approach for Faddeev equations. We introduce a new representation for Merkuriev boundary conditions and apply the complex-scaling method for obtaining the zero boundary value problem for Faddeev equations.

In the first approach [3], the asymptotic boundary conditions are represented in the form of the hyperspherical adiabatic expansion. This expansion is constructed in such a way that the binary and breakup channels are orthogonal at any value of the hyper-radius. This property allows using the asymptotic value of the Faddeev component as the boundary value [4] for the Faddeev equation. This approach makes it possible to calculate scattering parameters at the asymptotic region through the solution of the boundary value problem with the inhomogeneous boundary conditions in the asymptotic region, i. e. without reconstruction of the solution in the entire configuration space.

The second approach is to take advantage of the exterior complex-scaling method [5] for the inhomogeneous Faddeev equations. The method allows us to reduce the asymptotic boundary conditions to the homogeneous zero conditions at large separation of particles by the rotation of the hyper-radius into the upper complex half-plane. This approach demands calculation of the integral representation [1, 6] for scattering amplitudes. Therefore, it needs the reconstruction of the full solution over the entire configurational space.

The numerical solution of the problem includes solving the linear systems of equations with block tridiagonal matrices of large orders. The matrix sweeping algorithm [7] is a traditional computational scheme for such problems. Despite the fact that the algorithm is well defined and robust for matrices with diagonal dominance its recursive nature leads to a negative effect for taking advantage of parallel computers for large matrices. For our first approach, we use a technically simple scheme of matrix sweeping algorithm for forward elimination step which produces the solution only at the asymptotic region. For the second approach which requires the complete solution, we have to take advantage of parallel algorithms and to perform calculations using supercomputing facilities. In this case, the sweeping algorithm is applicable only as a brute-force algorithm due to its hard parallelization. For this case we have developed a new domain decomposition method (DDM). Using DDM on the supercomputer cluster allows us to reduce the computation time by an order of magnitude comparing to the brute-force algorithm.

The developed algorithms include conventional linear algebra packages as LAPACK and principal implementations of parallel programming concepts. The scattering amplitudes obtained by both approaches have been compared against each other and with results in [8].

The plan of the paper is as follows. In the second section a brief formulation of the three-body scattering problem is presented. The third section describes methods of solving the stated problem. The equations and the corresponding boundary conditions for each of approaches are given here. The computational methods as well as its parallelization are discussed in the fourth section. The obtained results are summarised and compared in the last fifth section before the conclusion.

The authors are thankful to E. A. Yarevsky for valuable suggestions concerning the application of the complex-scaling method. All calculations presented in the paper have been performed using the supercomputing facilities of the Computational Resources Center of SPbSU.

2 Formulation of the problem

The *nd* system under consideration is described by differential Faddeev equation of the form [1]

$$(-\Delta + V(\mathbf{x}) - E)\, U(\mathbf{X}) = -V(\mathbf{x})\left(P^+ + P^-\right) U(\mathbf{X}) \tag{1}$$

for the Faddeev component U of the wave function Ψ. The center-of-mass frame of standard Jacobi coordinates $\{\mathbf{x}, \mathbf{y}\} = \mathbf{X}$ [1] is used throughout. The expansion of the wave function into components is written as

$$\Psi(\mathbf{X}) = \left(I + P^+ + P^-\right) U(\mathbf{X}),$$

where $P^{\pm}$ is the cycling and anti-cycling permutation operators of three particles and I is the unit operator. The s-wave equations for the radial part of the Faddeev wave function component appear from the equation (1) after projection onto the states with zero orbital momentum in all pairs of the three-body system. These s-wave Faddeev equations are given by [9]

$$\left(-\frac{\partial^2}{\partial x^2} - \frac{\partial^2}{\partial y^2} + V^J(x) - E\right) U^J(x,y) = -V^J(x) \int\limits_{-1}^{1} d\mu \frac{xy}{x'y'} \mathbf{B}^J U^J(x',y'), \tag{2}$$

where

$$x' = \left(\frac{x^2}{4} - \frac{\sqrt{3}}{2} xy\mu + \frac{3y^2}{4}\right)^{1/2},$$

$$y' = \left(\frac{3x^2}{4} + \frac{\sqrt{3}}{2} xy\mu + \frac{y^2}{4} \right)^{1/2},$$
$$\mu = \cos(\hat{x}, \hat{y}).$$

The superscript J labels states with a given total momentum that coincides with the total spin of the system in our case. For $J = 1/2$ (doublet), $U^{1/2}$ is a three-component function $\left(U_1^{1/2}, U_2^{1/2}, U_3^{1/2}\right)^T$, whereas $U^{3/2}$ is a scalar (quartet). The potentials are defined as follows: $V^{1/2} = \mathrm{diag}\{V^t, V^s, V^s\}$, $V^{3/2} = V^t$, where V^t and V^s are triplet and singlet potentials of NN-interaction [8]. Numerical matrices $\mathbf{B}^J$ are given as

$$\mathbf{B}^{1/2} = \begin{pmatrix} 1/4 & -3/4 & 0 \\ -3/4 & 1/4 & 0 \\ 0 & 0 & -1/2 \end{pmatrix}, \quad \mathbf{B}^{3/2} = -1/2.$$

The energy E in the center-of-mass system and the relative neutron momentum q are associated with the deuteron ground state energy $\varepsilon < 0$ by the equation $q^2 = E - \varepsilon$. The deuteron ground state wave function satisfies the equation

$$\left(-\frac{d^2}{dx^2} + V^{3/2}(x) \right) \varphi(x) = \varepsilon \varphi(x) \tag{3}$$

with the zero boundary conditions at zero and infinity.

The solution of the s-wave Faddeev equations (2) for nd scattering above the breakup threshold ($E > 0$) should satisfy the boundary conditions [2]

$$U_1^{1/2}(x, y) \sim \varphi(x) \left(\sin qy + a_0^{1/2}(q) \exp iqy \right) + A_1^{1/2}(\theta, E) \frac{\exp i\sqrt{E}\rho}{\sqrt{\rho}}, \tag{4}$$

$$U_i^{1/2}(x, y) \sim A_i^{1/2}(\theta, E) \frac{\exp i\sqrt{E}\rho}{\sqrt{\rho}}, \quad i = 2, 3, \tag{5}$$

$$U^{3/2}(x, y) \sim \varphi(x) \left(\sin qy + a_0^{3/2}(q) \exp iqy \right) + A^{3/2}(\theta, E) \frac{\exp i\sqrt{E}\rho}{\sqrt{\rho}}, \tag{6}$$

where $\rho = \sqrt{x^2 + y^2}$, $\tan\theta = y/x$, as $\rho \to \infty$, and the conditions $U(x, 0) = U(0, y) = 0$ guarantee the regularity of the solution at zero. The structure of the numerical matrix $\mathbf{B}^{1/2}$ makes it possible to reject the third uncoupled equation in (2) and thus to simplify the problem. The functions $a_0^J(q)$ and $A_i^J(\theta, E)$ are the binary amplitude and the Faddeev component of the breakup amplitude, respectively. The integral representations for these functions in the simplest case $J = 3/2$ are of the form [1]

$$a_0^{3/2}(q) = \frac{1}{q} \int_0^\infty dy \, \sin qy \int_0^\infty dx \, \varphi(x) \, \mathcal{K}(x, y) \tag{7}$$

and

$$A^{3/2}(\tilde{\theta}, E) = \sqrt{\frac{2}{\pi\sqrt{E}}} e^{i\pi/4} \int_0^\infty dy \, \sin qy \int_0^\infty dx \, \phi(\sqrt{E}\cos\tilde{\theta}, x) \, \mathcal{K}(x, y), \tag{8}$$

where $\phi(k, x)$ is the scattering two-body wave function

$$\phi(k, x) \underset{x \to \infty}{\to} e^{i\delta(k)} \sin(kx + \delta(k))$$

and

$$\mathcal{K}(x, y) = \frac{1}{2} V^{3/2}(x) \int_{-1}^{1} d\mu \frac{xy}{x'y'} U^{3/2}(x', y').$$

Taking into account the change of the unknown function $\mathcal{U}^J(\rho,\theta) \equiv \sqrt{\rho}\,U^J(x,y)$, the transformation to the hyperspherical coordinates $\{\rho,\theta\}$ leads to the following equations:

$$\left(-\frac{\partial^2}{\partial\rho^2} - \frac{1}{4\rho^2} - \frac{1}{\rho^2}\frac{\partial^2}{\partial\theta^2} + V^{3/2}(\rho\cos\theta) - E\right)\mathcal{U}^{3/2}(\rho,\theta) = \frac{2}{\sqrt{3}}\,V^{3/2}(\rho\cos\theta)\int\limits_{\theta_-(\theta)}^{\theta_+(\theta)}\mathcal{U}(\rho,\theta')\,d\theta' \quad (9)$$

for $J = 3/2$ and

$$\left(-\frac{\partial^2}{\partial\rho^2} - \frac{1}{4\rho^2} - \frac{1}{\rho^2}\frac{\partial^2}{\partial\theta^2} + V^{t}(\rho\cos\theta) - E\right)\mathcal{U}_1^{1/2}(\rho,\theta) = -\frac{1}{\sqrt{3}}\,V^{t}(\rho\cos\theta)\int\limits_{\theta_-(\theta)}^{\theta_+(\theta)}\left(\mathcal{U}_1^{1/2}(\rho,\theta') - 3\,\mathcal{U}_2^{1/2}(\rho,\theta')\right)\,d\theta', \quad (10a)$$

$$\left(-\frac{\partial^2}{\partial\rho^2} - \frac{1}{4\rho^2} - \frac{1}{\rho^2}\frac{\partial^2}{\partial\theta^2} + V^{s}(\rho\cos\theta) - E\right)\mathcal{U}_2^{1/2}(\rho,\theta) = -\frac{1}{\sqrt{3}}\,V^{s}(\rho\cos\theta)\int\limits_{\theta_-(\theta)}^{\theta_+(\theta)}\left(-3\,\mathcal{U}_1^{1/2}(\rho,\theta') + \mathcal{U}_2^{1/2}(\rho,\theta')\right)\,d\theta' \quad (10b)$$

for $J = 1/2$. The integration limits are defined, in turn, as $\theta_-(\theta) = |\pi/3 - \theta|$, $\theta_+(\theta) = \pi/2 - |\pi/6 - \theta|$ and the boundary conditions (4)–(6) should be multiplied by $\sqrt{\rho}$.

3 The solution methods

3.1 The asymptotic approach

The equations (9)–(10) are solved via expansion of the unknown function in basis functions associated with the eigenvalue problem for the operator $h(\rho)$:

$$h(\rho)\phi_k(\rho|\theta) = \left(-\frac{1}{\rho^2}\frac{\partial^2}{\partial\theta^2} + V^J(\rho\cos\theta)\right)\phi_k(\rho|\theta) = \lambda_k^J(\rho)\phi_k(\rho|\theta), \quad \theta\in[0,\pi/2]. \quad (11)$$

The spectral properties of this operator [3] allow us to orthogonalize the binary and breakup scattering channels and hence to reformulate [3] the problem in such a way that the boundary conditions (4)–(6) can be represented as the following equivalent ones:

$$\mathcal{U}^{3/2}(\rho,\theta) \sim \phi_0(\rho|\theta)\left(\mathcal{Y}_0(q\rho) + a_0^{3/2}(q)\,\mathcal{H}_0(q\rho)\right) + \sum_{k=1}^{N_\phi}\phi_k(\rho|\theta)\,a_k^{3/2}(E)\,\mathcal{H}_k(\sqrt{E}\rho) \quad (12)$$

for $J = 3/2$, and

$$\mathcal{U}_1^{1/2}(\rho,\theta) \sim \phi_0(\rho|\theta)\left(\mathcal{Y}_0(q\rho) + a_0^{1/2}(q)\,\mathcal{H}_0(q\rho)\right) + \sum_{k=1}^{N_\phi} a_{1,k}^{1/2}(E)\,\phi_k(\rho|\theta)\,\mathcal{H}_k(\sqrt{E}\rho), \quad (13a)$$

$$\mathcal{U}_2^{1/2}(\rho,\theta) \sim \sum_{k=1}^{N_\phi} a_{2,k}^{1/2}(E)\,\phi_k(\rho|\theta)\,\mathcal{H}_k(\sqrt{E}\rho) \quad (13b)$$

for $J = 1/2$. Here $\mathcal{Y}_0(t)$ and $\mathcal{H}_k(t)$ are expressed by

$$\mathcal{Y}_0(t) = \sqrt{\frac{\pi t}{2}}\,\frac{Y_0(t) + J_0(t)}{\sqrt{2}},$$

$$\mathcal{H}_k(t) = \sqrt{\frac{\pi t}{2}}\,H^{(1)}_{2k}(t)\,\exp i\Big(\frac{\pi}{4} + \pi k\Big)$$

through Bessel functions J_0, Y_0 and Hankel functions of the first kind $H^{(1)}_k$ [10]. The Faddeev component of the breakup amplitude is expressed in this case as a linear combination

$$A^J_i(\theta, E) = \lim_{\rho\to\infty} A^J_i(\theta, E, \rho) = \lim_{\rho\to\infty} \sum_{k=1}^{N_\phi} a^J_{i,k}(E)\,\phi_k(\rho|\theta),$$

whereas the binary amplitude is given by $a^J_0(q)$.

The extraction of the coefficients $a^J_{i,k}$ of the presented linear combination, for example, in the case $J = 3/2$ is performed as follows. The boundary value problems with the boundary conditions given by separate terms of Eq. (12) and taken at some last knot $\rho_{max} + h$ are solved and the solutions $\mathcal{U}_k(\rho_{max})$ at the next-to-last knot are obtained. Parameter ρ_{max} is chosen to be large enough in order to use the asymptotic representation for the solutions in the asymptotic region. Constructing the complete solution as a linear combination

$$\mathcal{U} = \mathcal{U}_{\sin} + a_0^{3/2}\,\mathcal{U}_0 + \sum_{k=1}^{N_\phi} a_k^{3/2}\,\mathcal{U}_k, \tag{14}$$

we assume that in this asymptotic region $\rho = \rho_{max}$ the constructed solution (14) is equal to the asymptotics (12):

$$\mathcal{U}_{\sin} + a_0^{3/2}\,\mathcal{U}_0 + \sum_{k=1}^{N_\phi} a_k^{3/2}\,\mathcal{U}_k = \phi_0\left(\mathcal{Y}_0 + a_0^{3/2}\,\mathcal{H}_0\right) + \sum_{k=1}^{N_\phi} a_k^{3/2}\,\phi_k\,\mathcal{H}_k. \tag{15}$$

This provides the system of linear equations for calculation of $a_k^{3/2}$ in the asymptotic region, i. e. using the orthogonality of the basis and projecting Eqs. (15) on the basis functions ϕ_l, one can obtain the desired system of equations for $a_k^{3/2}$:

$$a_0^{3/2}\,[\langle\phi_l|\mathcal{U}_0\rangle - \langle\phi_l|\phi_0\mathcal{H}_0\rangle] + \sum_{k=1}^{N_\phi} a_k^{3/2}\,[\langle\phi_l|\mathcal{U}_k\rangle - \langle\phi_l|\phi_k\mathcal{H}_k\rangle] = -\langle\phi_l|\mathcal{U}_{\sin}\rangle + \langle\phi_l|\phi_0\mathcal{Y}_0\rangle.$$

3.2 The exterior complex-scaling method

The exterior complex-scaling method [5] implies a substitution of the variable ρ in Eqs. (9)–(10) by a complex function $R(\rho)$ according to the formula

$$R(\rho) = \begin{cases} \rho & \rho < \rho_0 \\ \rho_0 + f(\rho, \rho_0, \omega, \{p_i\}) & \rho \geq \rho_0 \end{cases},$$

where the introduced complex function f defines the curve of $R(\rho)$ in the complex plane and can depend on some number of predefined parameters p_i. Then the partial second derivative in equations (9)–(10) is expressed as

$$\frac{\partial^2}{\partial R^2} = -\frac{R''_\rho}{(R'_\rho)^3}\frac{\partial}{\partial\rho} + \frac{1}{(R'_\rho)^2}\frac{\partial^2}{\partial\rho^2}. \tag{16}$$

The continuity properties of $R(\rho)$ define the validity of Eq. (16) and the smoothness of the scaling. The simplest case of the sharp exterior complex-scaling demands to have f in the form

$$f(\rho, \rho_0, \omega, \{p_i\}) = (\rho - \rho_0)e^{i\omega}, \tag{17}$$

which prescribes the rotation to the upper complex half-plane by the angle ω. The derivative R'_ρ in this case has the discontinuity at ρ_0 and this might affect the applicability of the formula (16). A smooth exterior complex-scaling can be given by a more complicated function f which provides a continuity of function $R(\rho)$ together with the first and second derivatives. Nevertheless, the limiting behavior of f as $\rho \to \infty$ should have a form (17). For example, the function f for the smooth scaling can be given by

$$f(\rho, \rho_0, \omega, p) = (\rho - \rho_0)\ e^{i\omega}\ (1 - \exp[-p(\rho - \rho_0)]).$$

In the present work for this type of scaling we use fifth order polynomial function with some chosen coefficients.

The impact of the complex rotation on the asymptotics results in an exponential decrease of the scattered waves. For simplicity, we will consider the quartet asymptotics $\mathcal{U}^{3/2}$ and the sharp complex-scaling. In the hyperspherical coordinates the asymptotics (4) is given by the formula

$$\mathcal{U}^{3/2}(R, \theta) \sim \sqrt{R}\,\varphi(R\cos\theta)\left(\sin qy + a_0^{3/2}(q)\ \exp iqy\right) + A^{3/2}(\theta, E)\ \exp i\sqrt{E}R.$$

The sharp complex rotation of the binary scattered wave $\exp(iqR\cos\theta)$ produces the term

$$\exp(iq[\rho_0 + (\rho - \rho_0)\cos\omega]\sin\theta)\exp(-q(\rho - \rho_0)\sin\omega\sin\theta),$$

which exponentially vanishes as $\rho \to \infty$ and the angle of the rotation determines the rate of vanishing. The breakup scattered wave shows a similar behaviour. In contrast, the incoming wave $\sin(qR\cos\theta)$ does not vanish after the complex rotation. This wave is substracted from the asymptotics and consequently from the unknown solution. Hence, in the case of $J = 3/2$, the inhomogeneous equation

$$\left(-\frac{\partial^2}{\partial R^2} - \frac{1}{4R^2} - \frac{1}{R^2}\frac{\partial^2}{\partial\theta^2} + V(R\cos\theta) - E\right)\tilde{\mathcal{U}}^{3/2}(R, \theta)$$
$$- \frac{2}{\sqrt{3}}\,V(R\cos\theta)\int\limits_{\theta_-(\theta)}^{\theta_+(\theta)}\tilde{\mathcal{U}}^{3/2}(R, \theta')\,d\theta'$$
$$= \frac{2}{\sqrt{3}}\,V(R\cos\theta)\int\limits_{\theta_-(\theta)}^{\theta_+(\theta)}\sqrt{R}\,\varphi(R\cos\theta')\,\sin(qR\sin\theta')\,d\theta'.$$

for $\tilde{\mathcal{U}}^{3/2} = \mathcal{U}^{3/2} - \sqrt{R}\,\varphi(R\cos\theta')\sin(qR\sin\theta')$ with homogeneous zero boundary conditions

$$\tilde{\mathcal{U}}^{3/2}(R, \theta) \underset{\rho=0}{=} 0, \quad \tilde{\mathcal{U}}^{3/2}(R, \theta) \underset{\rho\to\infty}{=} 0$$

is obtained. The similar equations with vanishing zero boundary conditions can be obtained for the case $J = 1/2$.

Within a framework of this method, the binary and breakup amplitudes are calculated using the integral representations (7) and (8), respectively. The complete solution for all values of hyper-radius $\rho \in [0, \rho_{max}]$, where $\rho_{max} > \rho_0$, is reconstructed and a part of the solution at real values of $R(\rho)$ is then used for calculation.

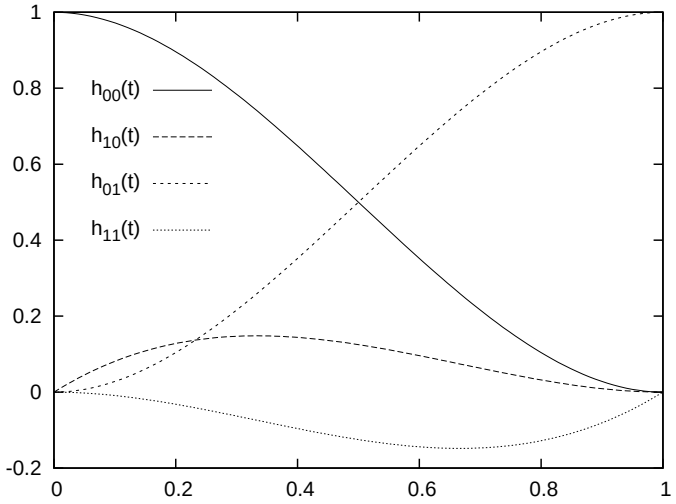

Figure 1: The cubic Hermite splines (18) at the unit interval.

4 The computational scheme

The two-dimensional boundary value problem is solved in the hyperspherical coordinates $\{\rho, \theta\}$ due to proper description of the boundary conditions and appropriate representation of the two-body operator (11). Therefore, the computational scheme meets the requirements of a good representation of this θ-dependent operator. As a result, the unknown solution as a function of the coordinate θ is expanded in the basis of cubic Hermit splines [11]. These four splines are defined at the unit interval by the formulae

$$\begin{array}{rcl} h_{00}(t) & = & 2t^3 - 3t^2 + 1, \\ h_{10}(t) & = & t^3 - 2t^2 + t, \\ h_{01}(t) & = & -2t^3 + 3t^2, \\ h_{11}(t) & = & t^3 - t^2, \end{array} \tag{18}$$

and can be transferred by linear transformations to two consecutive intervals of θ-grid. The splines are shown in Fig. 1. In order to obtain the θ-grid, a specially chosen nonequidistant x-grid for operator (3) has been used and transformed by the relation

$$\theta_i(\rho) = \arccos \frac{x_i}{X(\rho)}, \quad \theta_i \in [0, \pi/2].$$

Here the parameter $X(\rho)$ defines the x-coordinate of the right zero boundary condition for some ρ. The quality of the x-grid and consequently of the θ-grid has been estimated by a precision of the ground state eigenvalue of the two-body Hamiltonian (3). For the MT I-III potential [8], the achieved value is $E_{2b} = -2.23069$ MeV. The obtained nonequidistant θ-grid has the highest density near $\pi/2$ and makes it possible to calculate the precise ground state eigenvalue with about 500 intervals. The spline-expansion of the solution demands using as many as twice of numbers of coefficients in the expansion. The orthogonal collocation method with two gauss knots within one interval is used for discretisation of differential equations. Therefore, the common size for a matrix of the two-body operator representation is about 1000. The second partial derivative of the equation (9) is approximated over the equidistant ρ-grid with the mesh parameter $h = \rho_m - \rho_{m-1}$ by the finite-difference formula

$$\frac{\partial}{\partial \rho^2} \mathcal{U}(\rho, \theta) \to \frac{\mathcal{U}(\rho_{m-1}, \theta) - 2\,\mathcal{U}(\rho_m, \theta) + \mathcal{U}(\rho_{m+1}, \theta)}{h^2}.$$

This approximation generates the block tridiagonal structure for the matrix of the linear system. The matrix sweeping and the domain decomposition algorithms are

applied for solving the obtained system.

The matrix sweeping algorithm for the block tridiagonal system

$$\mathbf{A}_i X_{i-1} + \mathbf{C}_i X_i + \mathbf{B}_i X_{i+1} = S_i, \quad \mathbf{A}_1 = \mathbf{B}_{N_\rho} = 0, \tag{19}$$

where $\mathbf{A}_i$, $\mathbf{B}_i$, $\mathbf{C}_i$, $i = 1, \ldots, N_\rho$ are the blocks of the left hand side matrix and blocks S_i present the right hand side, includes two sweep procedures: the forward one and the backward one. The forward sweep consists of a sequential calculation of the auxiliary blocks

$$\begin{cases} \hat{\alpha}_1 &= \mathbf{C}_1^{-1}\mathbf{B}_1, \\ \hat{\alpha}_i &= \left(\mathbf{C}_i - \mathbf{A}_i\hat{\alpha}_{i-1}\right)^{-1}\mathbf{B}_i, \quad i = 2, ..., N_\rho - 1 \end{cases}$$

for the left hand side and similar ones for the right hand side. As a result, the matrix of the system is reduced using these blocks to the upper diagonal form with $\tilde{\mathbf{C}}_i$ blocks on the diagonal, unchanged $\mathbf{B}_i$ on the upper diagonal and $\tilde{S}_i$ in the right side. The backward sweep consists in the reconstruction of the solution of the linear system by formulae

$$\begin{cases} X_{N_\rho} &= \tilde{\mathbf{C}}_{N_\rho}^{-1}\tilde{S}_{N_\rho} \\ X_i &= \tilde{\mathbf{C}}_i^{-1}\left(\tilde{S}_i - \mathbf{B}_i X_{i+1}\right), \quad i = N_\rho - 1, \ldots, 1 \end{cases}$$

The solution is also calculated sequentially starting from the last block at the matrix diagonal. This makes it possible to calculate the solution corresponding to the last block by performing the complete forward sweep and only the first step of the backward sweep. In spite of its sufficient simplicity and efficiency, the matrix sweeping algorithm is recursive and parallelized only at the level of matrix operations. This does not allow us to use the given method on contemporary supercomputing facilities.

Besides the matrix sweeping algorithm, we have developed a new solution method called the domain decomposition method (DDM). It was designed to perform fast parallel solving and obtain a complete solution of the linear system. The idea of the method is presented in Fig. 2. The initial tridiagonal system (19) is rearranged into an equivalent form which allows the parallel solving. The matrix is logically divided into independent subsystems and last components of the solution corresponding to each subsystem are moved to the end of the full solution. The subsystems are shown in Fig. 2 (middle) by thin squares. This procedure affects the transformation of the initial matrix and reduces it to the new block "arrow"-form which is shown in Fig. 2 (bottom). The obtained system can be expressed as

$$\begin{pmatrix} \mathbf{M}_{11} & \mathbf{M}_{12} \\ \mathbf{M}_{21} & \mathbf{M}_v \end{pmatrix} \begin{pmatrix} u \\ v \end{pmatrix} = \begin{pmatrix} P_{11} \\ P_v \end{pmatrix}, \tag{20}$$

where the unknown solution v corresponds to the moved part of the full solution, the superblock $\mathbf{M}_{11}$ consists of the new independent blocks at the diagonal, $\mathbf{M}_v$ is the bottom right coupling superblock which is the "arrowhead", and other superblocks present additional blocks of the matrix. The solution of the system (20) is given by the relations

$$\begin{cases} u &= \mathbf{M}_{11}^{-1}\mathbf{P}_{11} - \mathbf{M}_{11}^{-1}\mathbf{M}_{12}v, \\ v &= \left(\mathbf{M}_v - \mathbf{M}_{21}\mathbf{M}_{11}^{-1}\mathbf{M}_{12}\right)^{-1}\left(P_v - \mathbf{M}_{21}\mathbf{M}_{11}^{-1}P_{11}\right). \end{cases}$$

Due to the structure of obtained superblocks, the inversion of $\mathbf{M}_{11}$ is reduced to independent inversions of the diagonal blocks corresponding to each subsystem. Only two nonzero blocks for each subsystem of $\mathbf{M}_{21}$ and $\mathbf{M}_{12}$ drastically reduce the number of matrix operations and their sparse allocation allows us to perform multiplications $\mathbf{M}_{11}^{-1}\mathbf{M}_{12}$ independently for each subsystem. The calculated supermatrix $\mathbf{M}_v - \mathbf{M}_{21}\mathbf{M}_{11}^{-1}\mathbf{M}_{12}$ has a block tridiagonal form. Although its size equals to the

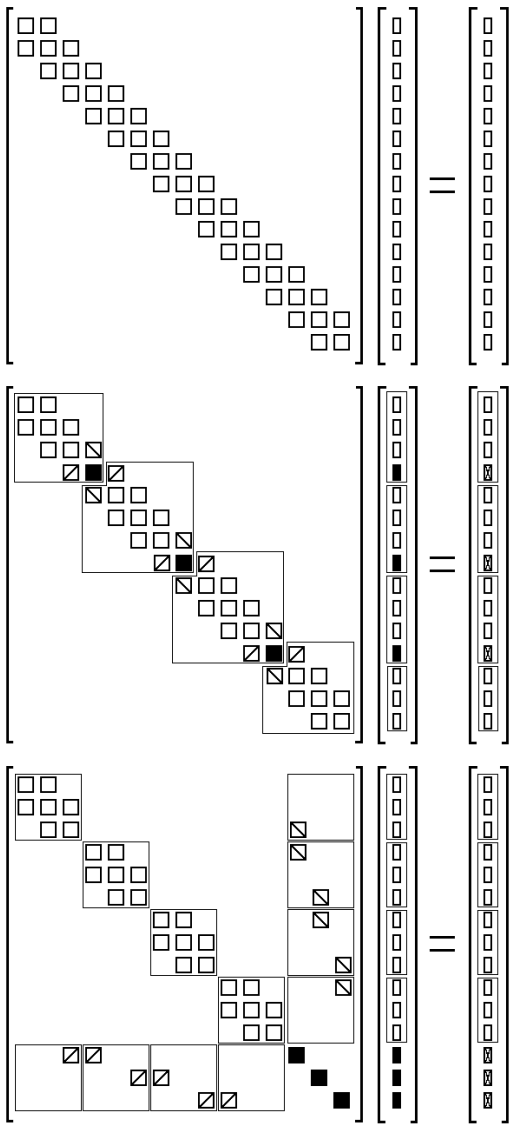

Figure 2: A simple graphical scheme of the domain decomposition method: (top) the initial block tridiagonal system; (middle) a rearrangement of the initial system to independent subsystems, the moved elements are highlighted by the diagonal lines and solid filling; (bottom) the obtained system in the "arrow"-form which can be solved using parallel calculations.

number of subsystems (multiplied by the size of one block) and can be chosen much smaller than the size of the initial system (19), the matrix sweeping algorithm is used for computation of the solution v. After obtaining v, the solution u is calculated in parts independently for each subsystem.

The DDM is successfully integrated in modern parallel programming models and it allows us to obtain a linear growth of performance with the increase of a number of computing units for not so large supercomputing systems. Fig. 3 shows obtained values of the computation acceleration with respect to the number of computing units. The linear dependence is clearly observed and the acceleration larger than 10 is easily reached. Nevertheless, further increase of computing hubs leads to violation of the linear dependence and stagnation of the performance increase because of the growth of hardly parallelized matrix sweeping part.

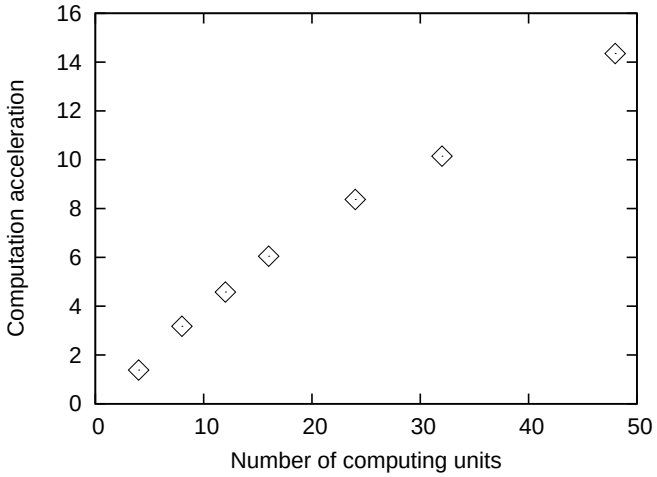

Figure 3: Computation acceleration for the domain decomposition method as a function of a number of computing units. The linear growth of the performance is observed.

5 Results of calculations

The calculations have been carried out for energies in the laboratory frame $E_{lab} = 14.1$, 42.0 MeV using the MT I-III potential [8] for the description of the two-body subsystem (3). A number of knots for the nonequidistant θ-grid was chosen to be about 1000 and the mesh step of the uniform ρ-grid was varied from 0.033 fm to 0.01 fm.

Within the asymptotic approach, the boundary value problems consisting of equations (9), (10) and boundary conditions (12), (13) taken at the hyper-radius $\rho = \rho_{max}$, have been solved. The expansion coefficients $a^J_{i,k}(E, \rho_{max})$ as functions of ρ_{max} have been calculated and used for reconstructing of the Faddeev component of the breakup amplitude

$$A^J_i(\theta, E, \rho_{max}) = \lim_{\rho\to\infty} A^J_i(\theta, E, \rho_{max}, \rho) = \lim_{\rho\to\infty} \sum_{k=1}^{N_\phi} a^J_{i,k}(E, \rho_{max})\, \phi_k(\rho|\theta).$$

The prelimiting doublet breakup amplitudes $A^{1/2}_i(\theta, E, \rho_{max}, \rho)$ for $E_{lab} = 14.1$ MeV at some finite value of ρ_{max} are shown in Fig. 4. The breakup amplitudes $A^{1/2}_i(\theta, E, \rho_{max})$ as $\rho \to \infty$ for the same energy are presented in Fig. 5. A convergence to a limit is explicitly guaranteed by properties of the functions $\phi_k(\rho|\theta)$. The limiting forms of these functions as $\rho \to \infty$ are known and they are smooth for $\theta \in [0, \pi/2]$:

$$\phi_k(\rho|\theta) \underset{\rho\to\infty}{\sim} \frac{2}{\sqrt{\pi}} \sin 2k\theta.$$

Therefore, in contrast to the prelimiting case, a smooth behavior of the breakup amplitudes near 90 degrees is observed.

The convergence of the binary amplitude $a_0(q, \rho_{max})$ and breakup amplitude $A^{3/2}_i(\theta, E, \rho_{max})$ as $\rho_{max} \to \infty$ has been obtained. For example, the ρ_{max}-dependence of the inelasticity coefficient and the phase shift, defined as

$$a^J_0 = \frac{\eta^J e^{2i\delta^J} - 1}{2i}, \tag{21}$$

for $J = 3/2$ are presented in Fig. 6. It is shown in the figure that the decrease of the mesh step h for the ρ-grid to 0.01 fm leads to obtaining of oscillating but significantly less biased values of the phase shift as ρ_{max} increases. The oscillations are vanishing as

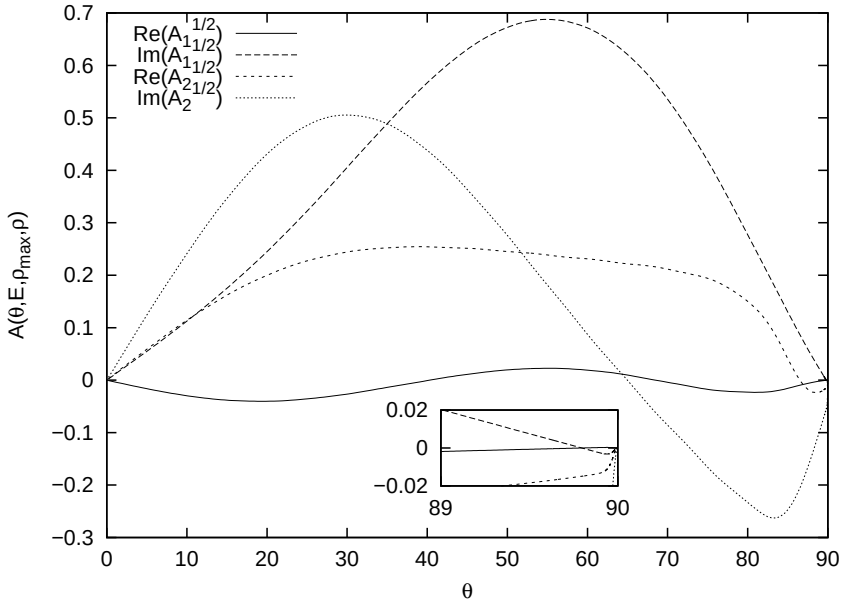

Figure 4: The prelimiting doublet breakup amplitudes $A_i^{1/2}(\theta, E, \rho_{max}, \rho)$ for $E_{lab} =$ 14.1 MeV and $\rho = \rho_{max} = 1400$ fm. The amplitudes have been obtained using the asymptotic approach.

$\rho_{max} \to \infty$ and the limiting value of the amplitude can be obtained by extrapolation. Nevertheless, in order to reach relatively small oscillations it is necessary to achieve values of $\rho_{max} > 1000$ fm. The obtained values of the binary amplitude for different laboratory frame energies are summarized in Table 1. The calculated values are in a good agreement with the binary amplitudes of Ref. [8].

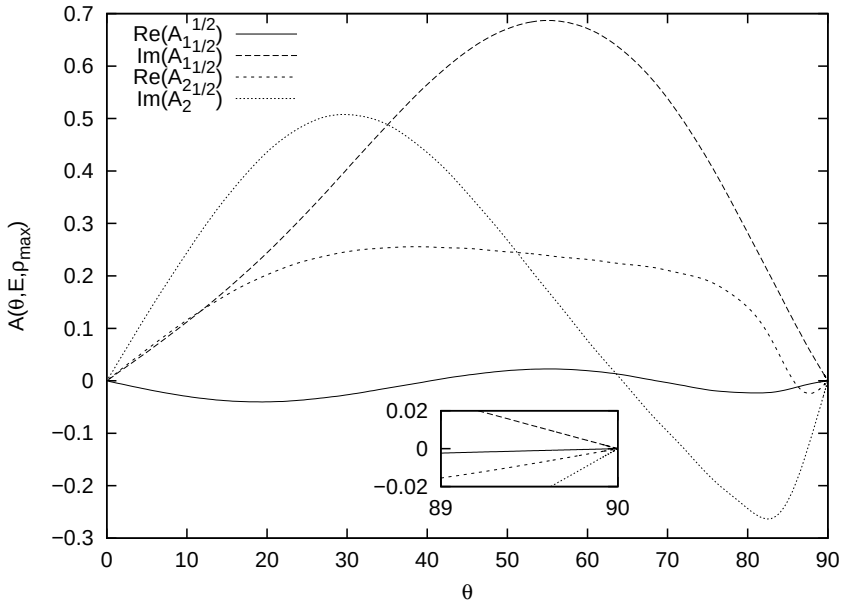

Figure 5: The breakup doublet amplitudes $A_i^{1/2}(\theta, E, \rho_{max})$ for $E_{lab} = 14.1$ MeV and $\rho_{max} = 1400$ fm. The amplitudes have been obtained using the asymptotic approach.

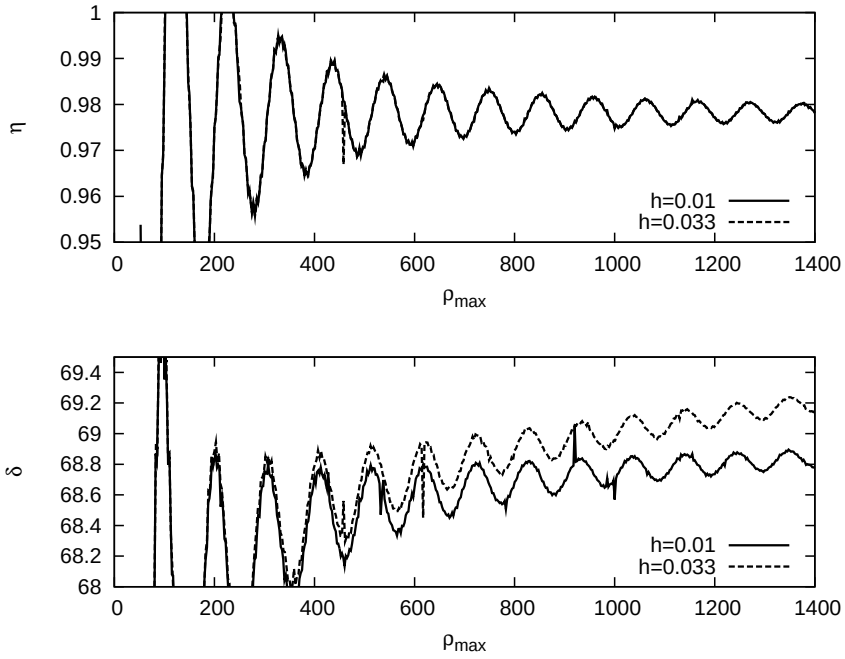

Figure 6: Calculated values of the quartet inelasticity coefficient η and phase shift δ [see Eq. (21)] for $E_{lab} = 14.1$ MeV as functions of ρ_{max}. The dashed line represents the values obtained using the ρ-grid with relatively large mesh $h = 0.033$ fm, whereas the solid line shows the values obtained using $h = 0.01$ fm. The values have been obtained using the asymptotic approach.

The complex-scaling approach calculations have been carried out using the smooth rotation by angle $\omega = 30°$ and mesh step of the ρ-grid $h = 0.033$ fm. Due to rotation, the boundary condition values have vanished and become smaller than 10^{-6}. The full solution was reconstructed and the amplitudes were calculated by the integral representations (7), (8). The most consistent preliminary values of the binary and breakup amplitudes have been obtained for the starting rotation at $\rho_{max} \sim 900$ fm and using the solution for $\rho_{max} < 900$ fm in formulae (7), (8). The achieved value of binary amplitude is expressed by the inelasticity coefficient $\eta = 0.9789$ and phase shift $\delta = 68.79°$. The obtained quartet breakup amplitudes $A^{3/2}(\theta, E, \rho_{max})$ were compared with the results of Ref. [8]. This comparison for $E_{lab} = 14.1$ MeV is presented in Fig. 7. The results are in good agreement for values of $\theta < 80°$, whereas differences are observed for $\theta \sim 90°$.

Table 1: The values of the inelasticity coefficient η and phase shift δ obtained using the asymptotic approach for different laboratory frame energies.

E_{lab}, MeV	14.1	42.0
$J = 3/2$, quartet		
$\eta^{3/2}$	0.9781	0.9031
$\delta^{3/2}$	68.78	37.66
$J = 1/2$, doublet		
$\eta^{1/2}$	0.4648	0.5021
$\delta^{1/2}$	105.40	41.21

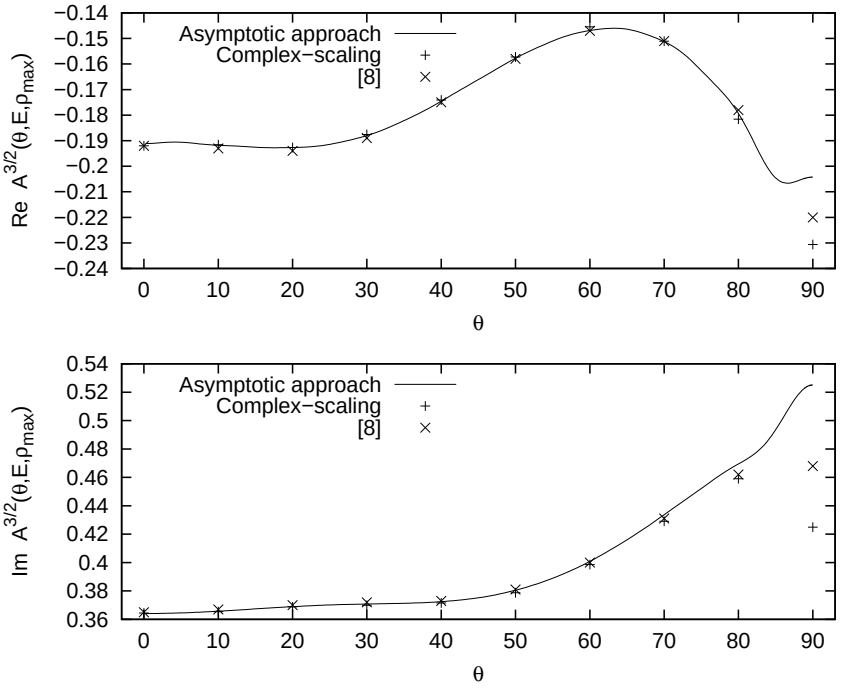

Figure 7: Real and imaginary parts of the breakup quartet amplitude $A^{3/2}(\theta, E, \rho_{max})$ for $E_{lab} = 14.1$ MeV. The values have been obtained using the asymptotic approach and the complex-scaling method. The results of Ref. [8] are also shown for comparison.

6 Conclusion

In the paper we have presented two methods for solving the three-body scattering problem above the breakup threshold. In the method 1, an orthonormal basis related to the two-body subsystem Hamiltonian is constructed. The asymptotic boundary condition is modified in terms of this basis. The breakup amplitude is represented by a linear combination of basis functions which allows an extrapolation of this amplitude to infinity exclusively by the properties of the basis functions. The coefficients of the linear combination together with the binary amplitude are numerically obtained from the comparison with the asymptotic form of the wave function. In the method 2, the exterior complex scaling is used for reducing the asymptotic boundary conditions to zero. The binary and breakup amplitudes are obtained from their integral representations. Both methods include solving the system of linear algebraic equations. The domain decomposition method which allows a parallelization of the solution process has been developed and successfully applied reducing the overall time of calculation up to 10 times.

References

[1] L. D. Faddeev and S. P. Merkuriev, *Quantum scattering theory for several particle systems*. Kluwer, Dordrecht, 1993.

[2] S. P. Merkuriev, C. Gignoux and A. Laverne, Ann. Phys. (NY) **99**, 30 (1976).

[3] P. A. Belov and S. L. Yakovlev, Bull. Russ. Acad. Sci. Phys. **76**, 913 (2012).

[4] P. A. Belov and S. L. Yakovlev, Vestnik St. Petersburg Univ., Ser. 4, 95 (2010).

[5] M. V. Volkov, N. Elander, E. A. Yarevsky and S. L. Yakovlev, Europhys. Lett. **85**, 30001 (2009).

[6] G. L. Payne, W. Glöckle and J. L. Friar, Phys. Rev. C **61**, 024005 (2000).

[7] A. A. Samarskiy and E. S. Nikolaev, *Methods for solving finite-difference equations*. Nauka, Moscow, 1978 (*in Russian*).

[8] J. L. Friar, G. L. Payne, W. Glöckle, D. Hüber and H. Witała, Phys. Rev. C **51**, 2356 (1995).

[9] S. L. Yakovlev and I. N. Filikhin, Phys. Atom. Nucl. **56**, 1676 (1993).

[10] M. Abramowitz and I. A. Stegun, *Handbook of Mathematical Functions with Formulas, Graphs, and Mathematical Tables*. Dover, New York, 1972.

[11] G. L. Payne in *Proc. 8th Autumn School Models and Methods Few-Body Phys., Lisboa, 1986*, edited by L. S. Ferreira *et al.* Springer-Verlag, Berlin, 1987, p. 64.